



Full paper / Mémoire

Structural variation in the copper(II) complexes with a tetradentate bis-6-methylpyridine-substituted bispidine ligand

Peter Comba*, Bodo Martin, Alexander Prikhod'ko, Hans Pritzkow, Heidi Rohwer

Anorganisch-Chemisches Institut der Universität Heidelberg, INF 270, 69120 Heidelberg, Germany

Received 6 May 2004; accepted 21 September 2004

Available online 20 April 2005

Abstract

Four single crystal X-ray structures of the complex cation $[\text{Cu}^{\text{II}}(\text{L})(\text{X})]^{n+}$ ($\text{L} = 3,7\text{-dimethyl-2,4-di-(6-methyl-2-pyridyl)-9-diol-3,7-diazabicyclo[3.3.1]nonane-1,5-dicarboxylate dimethylester}$, $\text{X} = \text{NCCH}_3, \text{OH}_2, \text{Cl}^-, \text{NO}_3^-$) are discussed together with their spectroscopic properties. The bispidine ligand L enforces a square pyramidal or *cis*-octahedral coordination geometry with two *cis*-disposed tertiary amines (N3 and N7), two *trans*-disposed pyridines which are co-planar and in-plane with the metal center and one of the two amines (N3), and one or two co-ligands *trans* to the amine donors (N3 or N7). Three structural types have been found: (i) $\text{X} = \text{NCCH}_3$, square pyramidal, X *trans* to N3 , in-plane with the pyridine donors, elongation of the Cu-N7 bond; (ii) $\text{X} = \text{Cl}^-, \text{OH}_2$, square pyramidal, X *trans* to N7 , perpendicular to the pyridine planes, slight elongation of the Cu-N3 bond; (iii) $\text{X} = \text{NO}_3^-$, octahedral, bidentate NO_3^- , elongation of the $\text{Cu-N}^{\text{pyridine}}$ bonds. The three isomeric chromophores ($\text{Cu}(\text{L})$ -fragments, the three possible minima of the 'Mexican hat' Jahn–Teller potential energy surface) are discussed on the basis of the experimental structural data, the steric contributions to the stabilization/destabilization of the three energetically similar minima are discussed on the basis of empirical force field calculations, and the results of DFT model calculations are used for a qualitative interpretation of electronic effects. Solid state and solution electronic spectra and frozen solution EPR spectra are used for a qualitative analysis of the three electronic ground states and a possible equilibration of the three isomeric forms, and this is supported by a preliminary ligand field analysis, based on AOM model calculations. **To cite this article: P. Comba et al., C R Chimie 8 (2005).**

© 2005 Académie des sciences. Published by Elsevier SAS. All rights reserved.

Résumé

Quatre structures déterminées aux rayons X de cristaux de complexes cationiques $[\text{Cu}^{\text{II}}(\text{L})(\text{X})]^{n+}$ ($\text{L} = 3,7\text{-diméthyl-2,4-di-(6-méthyl-2-pyridyl)-9-diol-3,7-diazabicyclo[3.3.1]nonane-1,5-dicarboxylate diméthylester}$, $\text{X} = \text{NCCH}_3, \text{OH}_2, \text{Cl}^-, \text{NO}_3^-$) sont examinées du point de vue de leurs propriétés spectroscopiques. Le ligand bispidine (L) contraint une géométrie pyramidale à base carrée ou une coordination octaédrique avec deux amines tertiaires *cis* (N3 et N7), deux pyridines *trans*, qui sont co-planaires et dans le plan du centre métallique et d'une des deux amines (N3), et un ou deux co-ligands en position *trans* par rapport aux amines (N3 ou N7). On a trouvé trois types structuraux (i) $\text{X} = \text{NCCH}_3$, pyramide à base carrée, X *trans* à N3 , dans le plan des pyridines, avec allongement de la liaison Cu-N7 ; (ii) $\text{X} = \text{Cl}^-, \text{OH}_2$, pyramide à base carrée, X *trans* à N7 , perpendiculaire aux

* Corresponding author.

E-mail address: peter.comba@aci.uni-heidelberg.de (P. Comba).

plans des pyridines, avec allongement de la liaison Cu–N3; (iii) X = NO₃[−], octaédrique, NO₃[−] bidentate, extension des liaisons Cu–N^{pyridine}. Les trois isomères chromophores (fragments Cu(L), les trois minima possibles de la surface d'énergie potentielle du « chapeau mexicain » de Jahn–Teller) sont examinés à partir des données structurales, tandis que les contributions stériques à la stabilisation/déstabilisation de trois minima énergétiquement similaires sont examinés sur la base de calculs empiriques des champs de force ; les résultats de modèles par calculs DFT sont utilisés dans l'interprétation des effets électroniques. La spectroscopie électronique à l'état solide ou en solution et la spectroscopie RPE en solution gelée sont utilisées pour l'analyse qualitative des trois états électroniques fondamentaux et la mise en évidence d'un possible équilibre des trois formes isomères, en s'appuyant sur une analyse préliminaire des champs des ligands à partir de modèles issus de calculs AOM. **Pour citer cet article : P. Comba et al., C R Chimie 8 (2005).**

© 2005 Académie des sciences. Published by Elsevier SAS. All rights reserved.

Keywords: Jahn–Teller distortion; Isomers; Mexican hat potential; Spectroscopy; DFT; Ligand field theory

Mots-clés: Distorsion de Jahn–Teller; Isomères; Potentiel de « chapeau mexicain »; Spectroscopie; DFT; Théorie du champ de ligands

1. Introduction

The bis-6-methylpyridine-substituted bispidine ligand L (L = 3,7-dimethyl-2,4-di-(6-methyl-2-pyridyl)-9-diol-3,7-diazabicyclo[3.3.1]nonane-1,5-dicarboxylate dimethylester, Fig. 1) is, in terms of the tertiary amine donors, a highly preorganized and very rigid ligand; the two pyridine donors are rotated away from the coordination site by approximately 180° but this torsion has a low energy barrier and, consequently, transition metal complexes with bispidine ligands generally are very stable [1,2]. However, due to a high elasticity of the coordination sphere, 3,4 bispidine ligands in general are less selective than might have been expected [1,3]. As a result of the elasticity a number of strikingly different structures of bispidine complexes have been observed, and these may be related to distortional isomerism [4–6]. A particularly interesting case is that of the hexacoordinate copper(II) complexes of a pentadentate bispidine derivative (two tertiary amine

and three pyridine donors, the third pyridine donor is a substituent of N3, acetonitrile as monodentate co-ligand), where two of the three possible directions of tetragonal elongation (along N7–Cu–N^{py3} and N^{py1}–Cu–N^{py2}) could be trapped and structurally characterized [5]. Here, we report single crystal structures, solid state and solution UV–vis–NIR and EPR data and a preliminary analysis, based on DFT, ligand field and force field calculations, of an example, where all three 'Jahn–Teller isomers' can be trapped. While, in the previous case [5], the reason for stabilization (destabilization) of one of the two minima was attributed to steric interactions exerted by the substituent at N7, in the example reported here, the relative stability of the three isomeric forms (with respect to the Cu(L)-fragment) is due to the mono- or bidentate co-ligand (NCCCH₃, OH₂, Cl[−], NO₃[−]), and steric as well as electronic effects may contribute to the stabilization of one of the three possible minima on the 'Mexican hat' potential energy surface.

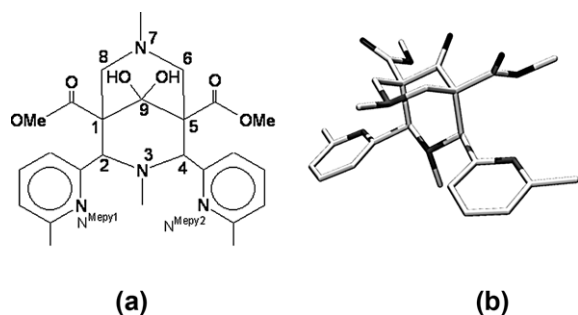


Fig. 1. (a) Structure of the bispidine ligand L, (b) (plot of the X-ray structure as the 9-keto derivative, hydrogen atoms omitted, N3...N7 = 2.867 Å [7]).

2. Experimental structural data

Two of the five structures discussed here (Fig. 2 and Table 1), i.e. [Cu(L)(NCCCH₃)](BF₄)₂·2CH₃CN (co-ligand *trans* to N3, elongated Cu–N7 bond) and [Cu(L)(Cl)](Cl)·CH₃CN (co-ligand *trans* to N7, Cu–N3 ≥ Cu–N7) have been reported before [7], that of [Cu(L)(OH₂)](BF₄)₂·H₂O also has the co-ligand *trans* to N7, and the two independent hexacoordinate structures with a chelating NO₃[−] ([Cu(L)(NO₃)](NO₃) have elongated Cu–N^{Mepy} bonds. The rigidity of the adamant-

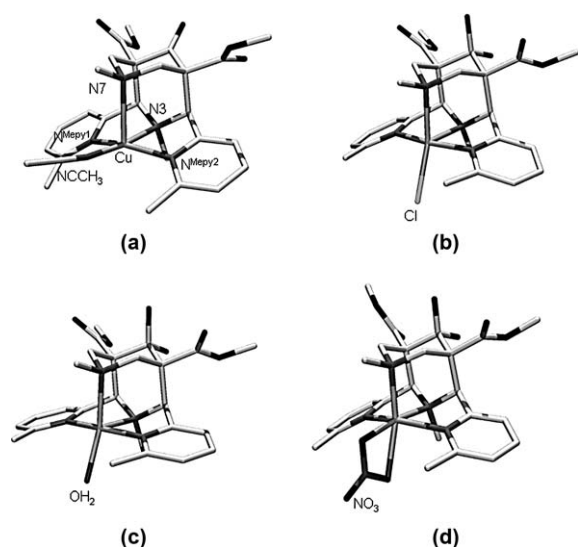


Fig. 2. Plots of the molecular cations of (a) $[\text{Cu}(\text{L})(\text{NCCH}_3)](\text{BF}_4)_2 \cdot 2 \text{CH}_3\text{CN}$ [7], (b) $[\text{Cu}(\text{L})(\text{Cl})]\text{Cl} \cdot \text{CH}_3\text{CN}$ [7], (c) $[\text{Cu}(\text{L})(\text{OH}_2)](\text{BF}_4)_2 \cdot \text{H}_2\text{O}$, (d) $[\text{Cu}(\text{L})(\text{NO}_3)]\text{NO}_3$ (hydrogen atoms omitted).

tanoide ligand backbone is shown by the constant N3...N7 distance of approximately 2.9 Å and an N3–Cu–N7 angle of approximately 85°. While these parameters are in the expected ranges [4], it appears that the bispidine ligands in the NO_3^- -structures, with the elongation along the $\text{N}^{\text{Mepy}1}\text{--Cu--N}^{\text{Mepy}2}$ axis, have a slightly larger than usual distortion. This seems to be an elegant way to compensate for an electronically enforced large $\text{N}^{\text{Mepy}1}\dots\text{N}^{\text{Mepy}2}$ distance by distribution of strain over a large part of the bispidine backbone. As shown below (Section 3) and in Table 1, the structural adjustment is primarily by low energy torsional distortions, and this leads to a minimum loss of energy. A considerable and unusual distortion is also observed for the structure with NCCH_3 as co-ligand, which has the quite generally observed square pyramidal geometry with the co-ligand in-plane and N7 as the axial donor. In order to minimize van der Waals repulsion with the 6-methyl substituents the NCCH_3 group is slightly bent up and the two pyridine rings are bent

Table 1
X-ray structural data of $[\text{Cu}(\text{L})\text{X}^1\text{X}^2]^{r+}$

	$[\text{Cu}(\text{L})(\text{NCCH}_3)](\text{BF}_4)_2 \cdot 2\text{CH}_3\text{CN}$ ^(a)	$[\text{Cu}(\text{L})(\text{Cl})]\text{Cl} \cdot 2\text{CH}_3\text{CN}$ ^(b)	$[\text{Cu}(\text{L})(\text{OH}_2)]^{2+}(\text{BF}_4)_2 \cdot \text{H}_2\text{O}$	$[\text{Cu}(\text{L})(\text{NO}_3)]\text{NO}_3$ ^(c)
Cu–N3	2.004 (0.004)	2.1474(0.0033)	2.1325(0.0012)	1.9763 (0.0015), 1.9866 (0.0016)
Cu–N7	2.376(0.004)	2.1200 (0.0033)	2.0869 (0.0012)	2.0919 (0.0015), 2.0318 (0.0016)
Cu–N ^{Mepy} 1	2.075 (0.004)	2.0614 (0.0033)	2.0293 (0.0012)	2.2586(0.0015), 2.3774(0.0018)
Cu–N ^{Mepy} 2	2.052 (0.004)	2.0640 (0.0032)	2.0153 (0.0012)	2.3467(0.0017), 2.3757(0.0018)
Cu–X ¹ (eq)	1.950 (0.005)	–	–	1.9638 (0.0016), 1.9819 (0.0015)
Cu–X ² (ox)	–	2.2208 (0.0015)	1.9907 (0.0012)	2.2828 (0.0019), 2.1391 (0.0018)
N3...N7	2.928	2.930	2.930	2.853, 2.834
Cu–N3/Cu–N7	0.84	1.01	1.02	0.94, 0.98
N3–Cu–N7	83.68 (0.14)	86.71 (0.12)	87.94 (0.04)	89.00 (0.06), 89.69 (0.06)
N3–Cu–X ¹	174.32 (0.17)	–	–	171.32 (0.06), 169.66 (0.06)
N7–Cu–X ²	–	160.3	161.60 (0.05)	159.49 (0.06), 163.35 (0.07)
N7–Cu–X ¹	90.9	–	–	99.63 (0.06), 100.56 (0.07)
N ^{Mepy} 1–Cu–N ^{Mepy} 2	155.62 (0.16)	163.82 (0.13)	165.60 (0.05)	155.61 (0.06), 152.54 (0.06)
N3–C–N ^{Mepy} 1	29.9	45.2	43.1	41.9, 41.7
N3–C–N ^{Mepy} 2	26.1	46.0	40.0	42.2, 44.8

^a Distances in Å, angles in °.

^b From [7].

^c Two independent X-ray structures.

down. This is nicely shown in the two torsional angles reported in Table 1. Due to the steric bulk of the pyridine methyl substituents, larger co-ligands (Cl^- , OH_2) are coordinated in the electronically less favorable position *trans* to N7 (see below and [8,9]). In the case of the bidentate NO_3^- there seems to be a subtle compromise between steric and electronic effects: the bidentate coordination mode does not allow for an elongation *trans* to N7 (note that significantly longer bonds *trans* to N7 than *trans* to N3, such as seen here in the NO_3^- structures, are generally observed and not only for Jahn–Teller-active systems [10,11]); therefore, the Cu–N7 bond is also relatively short (i.e. N7 is an in-plane donor, together with the other tertiary amine and the relatively weak oxygen donors of the chelating NO_3^-), and $\text{N}^{\text{Mepy1}}\text{–Cu–N}^{\text{Mepy2}}$ is the resulting Jahn–Teller axis. This also leads to relief of steric strain between the methyl substituents of the pyridine donors and the bidentate NO_3^- ligand.

3. Force-field calculations

Molecular mechanics was used to analyze the steric strain induced on the ligand by the electronically enforced elongation of one or two copper–donor bonds, and also for an analysis of the steric repulsion between the co-ligands (NCCH_3 , OH_2 , Cl^- , NO_3^-) and the bispidine backbone (primarily the 6-methyl substituents of the pyridine donors) in the three isomeric chromophores. Due to the use of a not fully refined ad-hoc copper–bispidine force field [4] and a number of additional approximations (see below), the results discussed here are not used for a quantitative assessment.

For the analysis of the ligand distortion the experimentally observed structures of $[\text{Cu}(\text{L})\text{X}]^{n+}$ with OH_2 , NCCH_3 and NO_3^- as co-ligands X were simplified (replacement of the ester groups at C1 and C5, and of the OH groups at C9 by hydrogen atoms; replacement of the co-ligands OH_2 and NCCH_3 by amine nitrogens, and of the bidentate NO_3^- by an NCN chelate) and optimized¹. The agreement between the experimental and optimized structures is acceptable, with respect to the ligand structures it is excellent. The co-ligands and cop-



Fig. 3. Overlay plot of the three structural forms of the ligand L, optimized by strain energy minimization of $[\text{Cu}(\text{L})\text{X}]^{n+}$ (see text); dark: Cl^- , OH_2 -structure, middle: NCCH_3 -structure, light: ONO_2^- -structure.

per(II) centers were then removed and the strain energies of the three optimized structures of the metal-free ligand, which correspond to the isomeric copper(II) chromophores, were determined by single-point calculations. These three steric energies of the ligand are similar; that resulting from the structure with the Jahn–Teller axis along $\text{N}^{\text{Mepy1}}\text{–Cu–N}^{\text{Mepy2}}$ (NO_3^- structure) is lowest (normalized to 0 kJ mol^{-1}), that with the elongation along Cu–N7 (NCCH_3 -structure) is less stable by 2.8 kJ mol^{-1} and that with the co-ligand *trans* to N7 (Cl^- , OH_2) and the elongation along Cu–N3 is the highest in energy (4.5 kJ mol^{-1}). As described above (Section 2), the similarity in terms of the steric energy was expected, and the bond stretch and valence angle distortions are minimal (e.g. the $\text{C}^{\text{Mepy}}\text{–C2(4)}\text{–C1(5)}$ angles are all within the range of $110.0\text{--}110.7^\circ$, i.e. practically constant and very close to the ideal sp^3 angle).

The major structural differences which emerge from Fig. 3 are, for the NCCH_3 -type structure (elongated Cu–N7 bond), a rotation of the pyridine rings such that the co-ligand lies above the pyridine planes and, more importantly, above the pyridine methyl substituents, and, for the NO_3^- -type structure with an elongation along the $\text{N}^{\text{Mepy1}}\text{–Cu–N}^{\text{Mepy2}}$ axis, a tilt of the bispidine backbone around the C2...C4 axis, coupled with the low-energy-barrier-adjustment of some torsional angles. Thus, primarily the structural changes of the Cu(L) chromophore involve a translation of the copper center within the bispidine cavity and the concomitant adjustment of the orientation of the pyridine donors by torsional distortions. Therefore, it is not unexpected that the strain induced onto the ligand in the three structures is small. This is also in agreement with the general observation with bispidine ligand complexes, that

¹ An optimization is required to reach the energy minimum on the potential energy surface, defined by the force field, which corresponds to the conformation given by the starting coordinates.

the potential energy surfaces are flat and, therefore, the coordination geometries are highly elastic [3–5,12].

The steric repulsion between co-ligands (NCCH_3 , OH_2 , Cl^- , NO_3^-) and the pyridine methyl substituents in the three isomeric forms was probed by addition of these donors to the three optimized isomeric Cu(L) -fragments in the crystallographically determined positions and orientations, followed by single-point calculations of the steric energies. For the two isomers with elongated Cu-N7 or Cu-N3 and short $\text{Cu-N}^{\text{Mepy}}$ bonds the experimentally observed coordination sites for the corresponding ligands (NCCH_3 *trans* to N3, OH_2 and Cl^- *trans* to N7) lead to the smallest van der Waals repulsion energies in the corresponding set of structures ($<40 \text{ kJ mol}^{-1}$), repulsion in the other sites is considerably higher ($>50 \text{ kJ mol}^{-1}$; the only structural parameters which were allowed to adjust in these calculations were rotations of the methyl groups). Interestingly, the geometry with an elongated $\text{N}^{\text{Mepy1}}\text{-Cu-N}^{\text{Mepy2}}$ axis tolerates not only NO_3^- but also the other co-ligands (NCCH_3 , OH_2 , Cl^-) with similar or even significantly lower repulsion than in the experimentally observed structural types (only large donors, such as Cl^- , when coordinated *trans* to N3 in this isomer lead to a significant but not excessive build-up of van der Waals repulsion). While the isomer with a long $\text{N}^{\text{Mepy1}}\text{-Cu-N}^{\text{Mepy2}}$ axis is the expected minimum energy structure for steric reasons, this is not what is observed experimentally (see Section 2). This suggests that there are electronic factors which destabilize this geometry. This also emerges from the observation that the only other examples where this mode of distortion has been detected are hexacoordinate copper(II) complexes [1,5].

It appears that relatively strong axial donors, such as tertiary amines or pyridines, in particular when copper-donor bond elongation is restricted, as in examples where these apical donors are part of five-membered chelate rings or where hexacoordination requires long axial bonds, lead to a quenching of the Jahn–Teller stabilization [5,6,9]. From experimental thermodynamic data (stability constants and redox potentials) [1,2,9,13] and model DFT calculations [8] the partial quenching of the Jahn–Teller stabilization is believed to lead to a loss of approximately $5\text{--}15 \text{ kJ mol}^{-1}$ [6]. With a chelating NO_3^- there seems to be a subtle balance between two electronically unfavorable ground states, as well as repulsive forces between the two methyl groups and the co-ligand.

4. Experimental spectroscopic data

Diffused reflectance electronic spectra of $[\text{Cu(L)(OH}_2)](\text{BF}_4)_2 \cdot \text{H}_2\text{O}$, $[\text{Cu(L)(NO}_3)]\text{NO}_3$ and $[\text{Cu(L)(Cl)}]\text{Cl} \cdot \text{CH}_3\text{CN}$ as well as solution spectra in various media are shown in Fig. 4. The solution spectra recorded in pure H_2O and, in particular, those at high Cl^- and NO_3^- concentration seem to indicate that the structures in these solutions are identical to those of the $[\text{Cu(L)(OH}_2)]^{2+}$, $[\text{Cu(L)(Cl)}]^+$ and $[\text{Cu(L)(NO}_3^-)]^+$ molecular cations, which are known from experiment. The electronic transitions of these chromophores and those in other solvent/salt mixtures, also shown in Fig. 4, are listed in Table 2. Solution EPR spectra of $[\text{Cu(L)(OH}_2)]^{2+}$ in various media are presented in Fig. 5; the corresponding spin Hamiltonian parameters are also given in Table 2.

The experiments in solution were complicated by the necessity to use specific solvent mixtures for the EPR spectra, in order to obtain good glasses and anisotropic spectra with well resolved hyperfine coupling; for comparison identical solvent mixtures were also used for electronic spectroscopy. From the usual $\text{DMF}/\text{H}_2\text{O}$ mixed solvent at various ratios it became clear that DMF coordination may also be involved². EPR spectra were also recorded in dry methanol and various solvent mixtures with methanol, H_2O , CH_3CN , $\text{C}_2\text{H}_5\text{CN}$ and DMF in various ratios. From this series of experiments it emerges that the spectra presented in Fig. 5 only involve one co-ligand X each (NCCH_3 , OH_2 , Cl^- , NO_3^-). From the spectrum with $\text{X} = \text{H}_2\text{O}$ in particular it therefore appears that two species are involved. The spin Hamiltonian parameters for both were obtained by spectra simulations [14,15] and these are given in Table 2, the simulated spectra are also presented in Fig. 5. From this it emerges that the solution electronic spectrum in Fig. 4a ($\text{X} = \text{OH}_2$) is not due to the same single species as that of the solid. However, due to the fact that the electronic transitions are broad, as usual, it is not possible to attribute specific features in the UV–NIR spectra to specific and different species in solution. The minor components of the other EPR spectra ($\text{X} = \text{CH}_3\text{CN}$, Cl^- , NO_3^-) are less well defined, and, consequently, the corresponding spin Hamiltonian parameters are less accurate and not unambiguous.

² DMF coordination is not discussed here in detail; even in dry DMF there are at least two species present, and these could be ‘Jahn–Teller isomers’, but probably linkage isomerism is also involved.

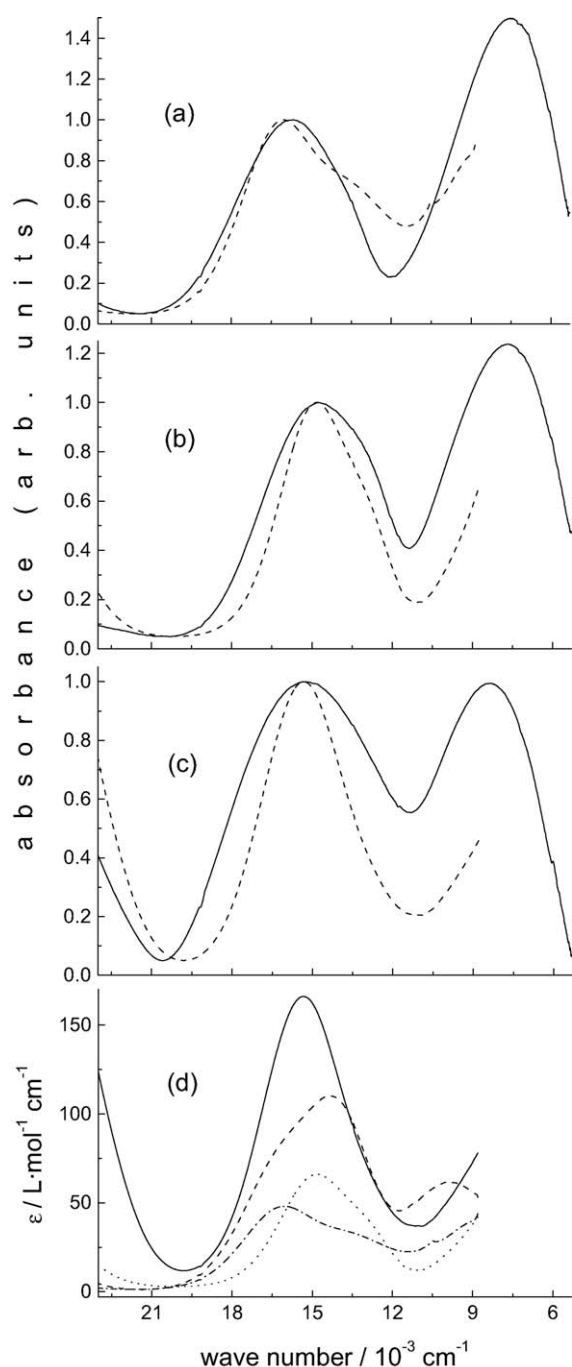


Fig. 4. Electronic spectra of $[\text{Cu}(\text{L})(\text{X})]^{2+}$. (a) $\text{X} = \text{H}_2\text{O}$, — solid, --- solution (pure H_2O); (b) $\text{X} = \text{NO}_3^-$, — solid, --- DMF, 0.25 M $\text{N}(\text{Bu})_4\text{NO}_3$; (c) $\text{X} = \text{Cl}^-$, — solid, --- solution DMF, 0.25 M $\text{N}(\text{Bu})_4\text{Cl}$; (d) — $\text{X} = \text{Cl}^-$: DMF, 0.25 M $\text{N}(\text{Bu})_4\text{Cl}$; --- $\text{X} = \text{CH}_3\text{CN}$: pure CH_3CN ; ... $\text{X} = \text{NO}_3^-$: DMF, 0.25 M $\text{N}(\text{Bu})_4\text{NO}_3$; - · - · - $\text{X} = \text{H}_2\text{O}$: pure H_2O .

Tetragonal ligand fields in copper(II) (square pyramidal or elongated octahedral) split the d-orbitals such that there is a $d_{x^2-y^2}$ ground state (unpaired electron in the $d_{x^2-y^2}$ orbital). In the AOM (angular overlap model) formalism [16] this is at an energy of $3e_\sigma$ (in-plane donors). The lowest energy transition may be assigned to that from the d_z -orbital at e_σ . The energy of this orbital is decreased by configurational interaction with the Cu 4s-orbital (ds-mixing, $e_\sigma - e_{ds}$, $e_{ds} \sim e_\sigma/4$) [17], and increased by the coordination of axial ligands ($e_\sigma - e_{ds} + e_\sigma^{\text{axial}}$). Therefore, in the bispidine complexes discussed here, with strong axial interactions, the $d_z \rightarrow d_{x^2-y^2}$ transition is expected at relatively low energies. From the solid state spectra it follows that the energy of this transition is in the order $\text{NO}_3^- \sim \text{OH}_2 < \text{Cl}^- \ll \text{NCCH}_3$, and this is as expected since in the NCCH_3 structure the axial donor (N7) has the smallest interaction (longest axial bond, see above, the NO_3^- structure has two axial donors) in the whole set of structures. The d_{xy}, xz, yz set of orbitals are only influenced by π -interactions ($d_{xy}: 4e_\pi; d_{xz}, yz: 2e_\pi + 2e_\pi^{\text{axial}}$). Therefore, with axial donors with little or no π -interaction the two highest energy transitions ($d_{xz, yz} \rightarrow d_{x^2-y^2}$, $d_{xy} \rightarrow d_{x^2-y^2}$) are expected to be split when in-plane π -donors are present, with axial π -interactions, this is reduced.

From the EPR spectra it appears that there are two sets of structures, i.e. those with relatively large A_{\parallel} hyperfine coupling (approximately $160\text{--}170 \cdot 10^{-4} \text{ cm}^{-1}$; $\text{X} = \text{NCCH}_3, \text{Cl}^-, \text{OH}_2$ first component, NO_3^- minor species) and those with relatively small A_{\parallel} values (approximately $140 \cdot 10^{-4} \text{ cm}^{-1}$, $\text{X} = \text{NO}_3^-$ major species, OH_2 second component, minor species in spectra with $\text{NCCH}_3, \text{Cl}^-$). There are semi-empirical methods to relate the hyperfine parameters to the in-plane and axial ligand fields [17], and corresponding qualitative predictions are in agreement with the observation that the chromophore with $\text{X} = \text{NO}_3^-$ (weak in-plane interactions, two relatively short bonds to axial pyridine donors) has a small A_{\parallel} value; from the electronic spectra (see Fig. 4 and Table 2) it emerges that with the two oxygen donors in the highly distorted basal plane this complex has the smallest ligand field in the series. The fact that the second component in the spectrum with $\text{X} = \text{OH}_2$ has similar EPR parameters suggests that this is due to an isomer with OH_2 *trans* to N3 and a concomitant elongation of the $\text{N}^{\text{Mepy1}}\text{--Cu--N}^{\text{Mepy2}}$ axis

Table 2

Experimental electronic and EPR spectra of $[\text{Cu}(\text{L})(\text{NCCH}_3)]^{2+}$, $[\text{Cu}(\text{L})(\text{Cl})]^+$, $[\text{Cu}(\text{L})(\text{OH}_2)]^{2+}$ and $[\text{Cu}(\text{L})(\text{NO}_3)]^+$

	Electronic transitions (cm^{-1})		$g_{x,y}$	g_z	A_z (10^{-4} cm^{-1})
	$[\text{Cu}(\text{L})(\text{NCCH}_3)]^{2+}$	16 300 (sh)	14 300	2.062	2.245
$[\text{Cu}(\text{L})(\text{Cl})]^+$	15 300		2.082 ^a	2.185 ^a	145 ^a
			2.062 ^a	2.196 ^a	145 ^a
$[\text{Cu}(\text{L})(\text{OH}_2)]^{2+}$	16 100	13 700 (sh)	2.055	2.255	172
			2.066	2.322	142
$[\text{Cu}(\text{L})(\text{NO}_3)]^+$	14 800	13 100 (sh)	2.066	2.320	142
			2.095 ^a	2.254 ^a	165 ^a

^a Minor component; simulation of these additional features is not unambiguous but they fit the observed spectra accurately (see Fig. 5).

(this probably leads to the coordination of a second OH_2 -donor *trans* to N7 to complete the in-plane donor set). This also is in agreement with the molecular-mechanics-based analysis of the steric energies (see above). The minor species detected in the EPR spectra of solutions with $\text{X} = \text{NCCH}_3$ and $\text{X} = \text{Cl}^-$ might also be due to chromophores with elongated copper–pyridine bonds, that with $\text{X} = \text{NO}_3^-$ might have one or two monodentate NO_3^- donors. Note, however, that the simulation of these minor EPR signals is not unambiguous.

5. Ligand-field calculations

While the structural, computational and spectroscopic data discussed so far lead to a consistent picture, they rely on a rather speculative assignment of the spectroscopic parameters. Therefore, these were supported with AOM model calculations. While ligand field parameters are not strictly transferable, it has been shown that the calculation of electronic transition energies with a constant set of ligand field parameters, adjusted to differences in metal–donor distances by $1/r^6$, leads to reasonably accurate predictions, in particular for copper(II) systems [17]. Parameters for $\text{Cu}-\text{N}^{\text{amine}}$ and $\text{Cu}-\text{OH}_2$ were used before in similar studies [17–21], those for $\text{Cu}-\text{N}^{\text{Mepy}}$ and $\text{Cu}-\text{Cl}$ were adapted from published spectroscopic studies [22,23]; for the structures with $\text{X} = \text{NO}_3^-$ $\text{Cu}-\text{O}$ parameters of OH_2 were adapted to 1.3 the value for H_2O (note that this might underestimate the π -interactions), those for $\text{Cu}-\text{NCCH}_3$ were extrapolated from the parameters of amines and water, assuming that acetonitrile is a π -acceptor, and fitted to the electronic spectrum. While

fine-tuning of all the parameters on the basis of a larger set of spectroscopic and structural data might lead to more accurate predictions [17,21], the main purpose of the present study is to assign the electronic transitions to specific isomeric forms of the copper(II)–bispidine chromophores, and this is possible with the present ad-hoc parameter set (see Table 3). There are also methods to compute the g -tensor parameters with reasonable accuracy [17], but the experimentally determined g -values are not well enough defined in all structures (see above), and their variation is relatively small (see Table 2) and, therefore, this is not pursued here. The structural parameters for the AOM calculations are from the crystallographically determined coordinates, for those of $[\text{Cu}(\text{L})(\text{OH}_2)_2]^{2+}$ (‘second isomer’) the copper and bispidine-donor coordinates were from the experimental structure with $\text{X} = \text{NO}_3^-$, and the two OH_2 donors were set *trans* to N3 and N7 with $\text{Cu}-\text{O} = 1.98$ and 2.10 \AA , respectively. This structural assumption is confirmed by the experimental structural data of $[\text{Cu}(\text{L})(\text{OH}_2)]^{2+}$ (see above) and by a DFT structure optimization (see below).

As expected and observed experimentally, the chromophore with $\text{X} = \text{NCCH}_3$ has the strongest ligand field and the highest energy $d_{z^2} \rightarrow d_{x^2-y^2}$ transition. The calculated transition energies for $[\text{Cu}(\text{L})(\text{Cl})]^+$ and $[\text{Cu}(\text{L})(\text{OH}_2)]^{2+}$ are similar since the two complexes have similar structures and the two monodentate co-ligands have similar ligand field parameters. Two *cis*-disposed in-plane O-donors (NO_3^- structure) lead to a very low ligand field with a small splitting within the set of transition originating from the $d_{xy,xz,yz}$ orbitals (π -interactions with NO_3^- lead to an increase of this energy difference). Based on this analysis, the shoulder in the spectrum of the aqua complex at $13\,700 \text{ cm}^{-1}$ is primarily attributed to $[\text{Cu}(\text{L})(\text{OH}_2)_2]^{2+}$.

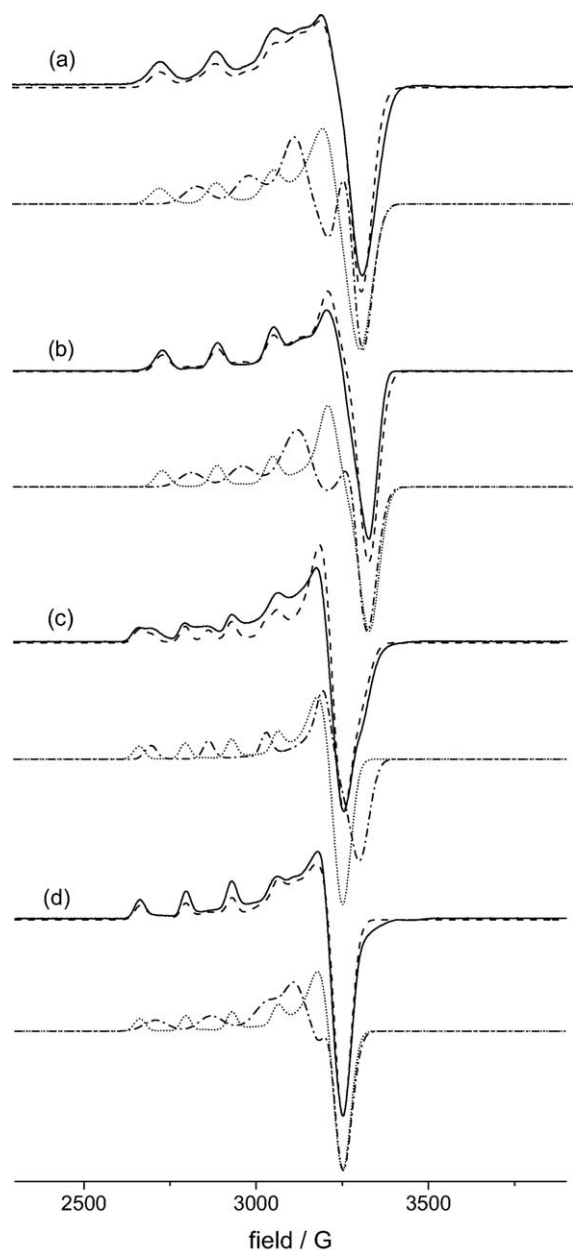


Fig. 5. Frozen solution EPR spectra of $[\text{Cu}(\text{L})(\text{X})]^{n+}$ (X-band, $T \sim 100$ K). (a) $\text{X} = \text{NCCH}_3$, $\text{CH}_3\text{CN}/\text{CH}_3\text{CH}_2\text{CN}$, 1:1; (b) $\text{X} = \text{Cl}^-$: DMF, 0.2 M $\text{N}(\text{Bu})_4\text{Cl}$; (c) $\text{X} = \text{OH}_2$, $\text{H}_2\text{O}/\text{DMF}$, 1:1; (d) $\text{X} = \text{NO}_3^-$, DMF, 0.25 M $\text{N}(\text{Bu})_4\text{NO}_3$; — experimental, --- simulation, ·····, ····· simulation of the two components each.

6. DFT calculations

For the structure optimizations based on approximate density functional theory a model was used, where

the ester groups at C1 and C5 were replaced by hydrogen atoms, and the $\text{C}(\text{OH})_2$ at C9 was replaced by $\text{C}=\text{O}$. The latter modification is based on the ligand originally used in the synthesis (the hydration product is usually observed when hydrous solvents are used [5,13], and it is known that the ketone leads to a decrease of the nucleophilicity of the amine donors [4,13,24]; this might be one of the reasons why all copper(II)–bispidine–donor bonds reported here are overestimated). Table 4 is a summary of the calculated structural parameters. The DFT calculations are able to qualitatively reproduce the experimental structures. Exceptions are the generally observed overestimated bond distances (see above) and the fact that the Jahn–Teller elongation is not well reproduced in two of the structures (see below). For the chromophores with $\text{X} = \text{Cl}^-$ and, specifically, for $\text{X} = \text{OH}_2$ the potential energy surface was searched in order to localize all local minimum structures and compare their stability. The corresponding data are also included in Table 4.

The structure with $\text{X} = \text{NCCH}_3$ is the only one which experimentally is observed with X *trans* to N3 and an elongated Cu–N7 bond. This is in good agreement with the DFT-based predictions. Specific distortions are also well reproduced, primarily the N3–C–C–N^{Mepy} torsional angles that allow the co-ligand X to move away from the pyridine–methyl substituents (this emerges also from the angular geometry of the chromophore, although these distortions are generally a little underestimated in the computed structures due to the overestimated bond distances). The good agreement between the computed and experimental structure is visualized in Fig. 6 (the difference in orientation of the NCCH_3 ligand is due to enforced C_s symmetry).

Local minima which correspond to the observed structure with $\text{X} = \text{NCCH}_3$ have also been found with the co-ligands $\text{X} = \text{Cl}^-$ and OH_2 . The three computed structures with elongated Cu–N7 bonds and in-plane co-ligands ($\text{X} = \text{NCCH}_3$, Cl^- , OH_2) are very similar to each other and confirm that these local minima are realistic (see Fig. 6). Molecular mechanics (see above) indicated that bulkier ligands than NCCH_3 lead to a build-up of steric strain (repulsion of the pyridine–methyl groups and the co-ligand). In agreement with this the DFT structures indicate that, for $\text{X} = \text{Cl}^-$ specifically, this strain leads to an elongation of the Cu–N^{Mepy} bonds see (Table 4). Spectroscopically, we have observed that, due to the resulting destabilization of this structural

Table 3

Calculated electronic spectra (experimental data in brackets) of $[\text{Cu}(\text{L})(\text{NCCH}_3)]^{2+}$, $[\text{Cu}(\text{L})(\text{Cl})]^+$, $[\text{Cu}(\text{L})(\text{OH}_2)]^{2+}$ and $[\text{Cu}(\text{L})(\text{NO}_3)]^+$

	Electronic transition (cm^{-1})			
$[\text{Cu}(\text{L})(\text{NCCH}_3)]^{2+}$	16 500 (16 300)	15 000 13 600	(14 300)	10 400 (10 000)
$[\text{Cu}(\text{L})(\text{Cl})]^+$	14 800 (15 300)	14 000 13 100	–	7100 (8300)
$[\text{Cu}(\text{L})(\text{OH}_2)]^{2+}$ ^a	15 500 (16 100)	14 200 13 500	(13 700)	7100 (7600)
	14 400 (13 700)	14 000 12 900		5700
$[\text{Cu}(\text{L})(\text{NO}_3)]^+$	14 500 (14 800)	14 000 13 100	(13 100)	6000 (7700)

^a Computed with two OH_2 donors in-plane with Cu, N3 and N7, Cu–O = 1.98 and 2.21 Å, respectively, elongated $\text{N}^{\text{Mepy}1}\text{–Cu–N}^{\text{Mepy}2}$ axis.

Table 4

Computed structures (DFT, B3LYP) of $[\text{Cu}(\text{L})(\text{X}^1)(\text{X}^2)]^{n+}$ ^{a,b}

	$[\text{Cu}(\text{L})(\text{NCCH}_3)]^{2+}$	$[\text{Cu}(\text{L})(\text{Cl})]^+$ ^c	$[\text{Cu}(\text{L})(\text{OH}_2)]^{2+}$ ^d	$[\text{Cu}(\text{L})(\text{NO}_3)]^+$
Cu–N3	2.029	<u>2.209</u> , 2.056	<u>2.143</u> , 2.013, 2.054	2.054
Cu–N7	<u>2.376</u>	2.216, <u>2.398</u>	2.239, <u>2.355</u> , 2.105	2.106
Cu– $\text{N}^{\text{Mepy}1}$	2.145	2.048, <u>2.205</u>	2.017, 2.138, <u>2.481</u>	<u>2.480</u>
Cu– $\text{N}^{\text{Mepy}2}$	2.145	2.048, 2.204	2.017, 2.138, <u>2.481</u>	<u>2.480</u>
Cu– X^1 (eq)	2.012	–, 2.212	–, 2.032, 2.050	2.005
Cu– X^2 (ax)	–	2.262, –	2.190, –, 2.277	2.118
N3...N7	3.029	3.024, 3.019	3.080, 3.028, 2.932	2.933
Cu–N3/Cu–N7	0.85	1.00, 0.86	0.95, 0.86, 0.98	0.98
N3–Cu–N7	86.5	86.2, 85.0	89.3, 87.4, 89.6	89.6
N3–Cu– X^1	179.1	–, 179.7	–, 179.9, 173.4	170.2
N7–Cu– X^2	–	166.9, –	163.5, –, 169.7	163.0
N7–Cu– X^1	92.6	–, 95.3	–, 92.5, 97.0	100.1
$\text{N}^{\text{Mepy}1}\text{–Cu–N}^{\text{Mepy}2}$	148.7	164.9, 146.9	166.2, 152.0, 149.6	149.7
N3–C– $\text{N}^{\text{Mepy}1}$	28.3	45.6, 26.2	43.3, 30.6, 44.2	44.1
N3–C– $\text{N}^{\text{Mepy}2}$	28.3	45.6, 26.2	43.3, 30.6, 44.2	44.1

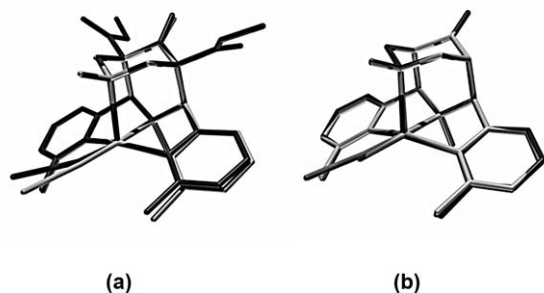
^a Distances in Å, angles in °.^b Underlined bond distances are the Jahn–Teller-elongated bonds observed experimentally.^c Two isomers; C1 *trans* to N7, *trans* to N3.^d Three isomers; OH_2 *trans* to N7, *trans* to N3 (OH_2)₂.

Fig. 6. Overlay plots of (a) the experimental and computed structures of $[\text{Cu}(\text{L})(\text{NCCH}_3)]^{2+}$ (dark: experimental, light: computed) and (b) the computed structures of $[\text{Cu}(\text{L})(\text{X})]^{n+}$ with an elongated Cu–N7 bond (X *trans* to N3) with X = NCCH_3 , middle, OH_2 , dark, Cl^- , light.

form, a switch to a second local minimum emerges, i.e. that with the Jahn–Teller axis along $\text{N}^{\text{Mepy}1}\text{–Cu–N}^{\text{Mepy}2}$. Probably, an additional OH_2 is then coordinated to complete the in-plane ligand field. This hexa-

coordinate structure with X = OH_2 has also been optimized with DFT (see Table 4). It is similar to that with the bidentate NO_3^- co-ligand and confirmed spectroscopically and by the AOM-computed transition energies (see above). The third structural form is that observed experimentally with X = Cl^- and OH_2 (see Table 1), with the monodentate co-ligand *trans* to N7 and an elongated Cu–N3 bond. The Cu–N3/Cu–N7 ratios in these structures are not well reproduced in the DFT-optimized geometries. Apart from some obvious and not unexpected deficiencies with respect to the energetics of the orbitals with large d-contributions (overestimated covalency of B3LYP calculations) this might also partially be due to the generally overestimated copper–donor bond distances (see above) and because N3 is part of a rigid five-membered chelate ring with little freedom to be significantly elongated. Energetically, the two five-coordinate local minimum structures (apical Cu–N7 or Cu–N3) are of similar sta-

bility with an energy difference of 5–10 kJ mol⁻¹ and the experimentally observed structure being less stable in both cases. With the relatively small energy differences and the structural inaccuracies discussed above the conclusion is that the two minima are close to degenerate and, as outlined above, this is in agreement with the spectroscopic data (e.g., EPR spectra of the aqua complex). This also confirms the general observation that bispidine-coordination compounds are highly elastic, i.e. they have flat potential energy surfaces with various local minima (three in the systems discussed here, and all have been found experimentally and localized by DFT calculations) [3–5,13].

7. Conclusions

Recently we have presented the first example of copper(II) complexes with asymmetrical ligands, where two of the three isomeric structures of the chromophore along a Jahn–Teller vibrational mode could be trapped [5]. We now are able to present an example where all three possible Jahn–Teller elongated structures are trapped and structurally as well as spectroscopically fully characterized. While in the earlier example, which also is based on bispidine ligands, the stabilization/destabilization of one of the two close to degenerate minima of the ‘Mexican hat’ potential energy surface was due to steric interactions (size of the substituent at N7) [5,25], in the [Cu(L)X]ⁿ⁺ systems presented here, the stability of either of the three minima is due to the size (steric interactions) and electronic properties of the co-ligand X. Experimentally determined solid state molecular structures and a combination of solid state and solution electronic and frozen solution EPR spectroscopy, combined with ligand field calculations and spectra simulations have helped to characterize the structural variation. Empirical force field and DFT calculations were used to determine the steric influence, and spectroscopy, ligand field and DFT calculations helped to analyze electronic influences. While each method alone has some deficiencies and weaknesses which lead to ambiguities, from the combination of all the data we arrive at a consistent picture.

8. Experimental section

8.1. Materials

Reagents and solvents were used without purification; L was prepared as described in [7].

[Cu(L)(NCCH₃)](BF₄)₂ and [Cu(L)(Cl)]Cl·H₂O were obtained as described before [7]. Solvents with quality grade ‘purum’ or ‘puriss’, tetrabutylammonium chloride (purum, ≥ 97%) and tetrabutylammonium nitrate (puriss, ≥ 99%) were used for spectroscopic measurements.

8.2. Syntheses

8.2.1. [Cu(L)(NO₃)](NO₃)

Cu(NO₃)₂·3 H₂O (0.78 g, 3.2 mmol) in water (10 ml) was added slowly to a suspension of L (1.5 g, 3.2 mmol) in methanol (30 ml). The resulting blue solution was put in a diethylether diffusion bath. After several days, blue crystals, suitable for X-ray diffraction precipitated from the solution (yield: 1.8 g, 2.7 mmol, 83%). C₂₅H₃₂N₆O₁₂Cu (672.10): Calcd. C 44.68, H 4.80, N 12.50; found C 44.27, H 4.81, N 12.25.

8.2.2. [Cu(L)(OH₂)](BF₄)₂·H₂O

[Cu(L)(NO₃)](NO₃) (1.2 g, 1.8 mmol) in water (0.5 l) was sorbed onto a SP-Sephadex C-25 cation exchange column (Na⁺ form). The column was washed with water (1 l), and the complex was eluted with 0.2 mol l⁻¹ NaBF₄. The eluate was concentrated to 25 ml and cooled to room temperature. The product was collected on a filter, washed with ethanol and dried in air (yield: 1.3 g, 1.7 mmol, 96%). C₂₅H₃₆N₄O₈CuB₂F₈ (757.73): Calcd. C 39.63, H 4.79, N 7.39; found C 39.66, H 4.81, N 7.36. Crystals suitable for X-ray diffraction were obtained by slow evaporation of the aqueous solution, saturated with NaBF₄.

8.3. Measurements

UV–vis–NIR spectra were measured on a Cary IE spectrophotometer (solutions) or a JASCO V-570 UV/VIS/NIR instrument (diffused reflectance, polytetrafluoroethylene pellets). EPR spectra were obtained with a Bruker ELEXSYS E500 spectrometer (X-band) from frozen solutions (110 K), the same solutions were also used for UV–vis–NIR spectroscopy. The EPR spectra were simulated by XSophe (Bruker) [14,15].

8.4. Crystal structure determination

Reflections of single crystals were measured with a Bruker AXS SMART 1000 diffractometer with Mo K α

Table 5

Crystallographic data of the X-ray diffraction studies

	[Cu(L)(OH ₂)](BF ₄) ₂ ·H ₂ O	[Cu(L)(NO ₃)]NO ₃	[Cu(L)(NO ₃)]NO ₃ ·1/2(CH ₃ OH)
Empirical formula	C ₂₅ H ₃₆ B ₂ Cu F ₈ N ₄ O ₈	C ₂₅ H ₃₂ Cu N ₆ O ₁₂	C _{25.50} H ₃₄ Cu N ₆ O _{12.50}
Formula weight	757.74	672.11	688.13
Temperature	103 (2)	298 (2)	103 (2)
Crystal system	Triclinic	Monoclinic	Triclinic
Space group	<i>P</i> $\bar{1}$	<i>P</i> 2 ₁ / <i>c</i>	<i>P</i> $\bar{1}$
<i>a</i> (Å)	11.3822 (6)	16.1439 (7)	11.4300 (4)
<i>b</i> (Å)	11.7737 (7)	13.3029 (6)	12.1400 (5)
<i>c</i> (Å)	12.1129 (7)	13.6704 (6)	13.3298 (5)
α	105.9270 (10)	90	78.773 (7)
β	97.7390 (10)	93.3430 (10)	64.815 (7)
γ	92.9380 (10)	90	62.433 (7)
<i>V</i> (Å ³)	1540.08 (15)	2930.9 (2)	1483.78 (10)
<i>Z</i>	2	4	2
<i>d</i> _{calc} (g cm ⁻³)	1.634	1.523	1.540
Absorbance coefficient (mm ⁻¹)	0.812	0.818	0.811
<i>F</i> (000)	778	1396	716
Crystal size (mm)	0.33 × 0.24 × 0.09	0.40 × 0.35 × 0.19	0.35 × 0.35 × 0.20
Theta max	32.02	30.50	32.00
Reflections			
Collected	27,387	25,781	17,698
Independent	10 465[0.0303]	8909 [0.0289]	9826[0.0205]
Parameters	603	525	473
GOF on <i>F</i> ²	1.043	1.015	1.044
<i>R</i> ₁ [<i>I</i> > 2σ(<i>I</i>)]	0.0362	0.0400	0.0518
<i>wR</i> ₂ (all data)	0.0993	0.1200	0.1566
Largest difference in peak/hole (e Å ⁻³)	0.821/−0.673	0.464/−0.295	1.711/−0.592

radiation ($\lambda = 0.71073$ Å) and operating in the ω -scan mode. The absorption correction was applied in all cases. The structures were solved by direct methods (SHELXS86) and refined by full-matrix, least-squares methods based on *F*² (SHELXL97), with use of anisotropic thermal parameters for all non-hydrogen atoms. Crystallographic data for the new structures in this paper are reported in Table 5 and the structural data have been deposited at the Cambridge Crystallographic Data Center (CCDC 243386, 243387, 243388).

Molecular mechanics calculations were done with the MOMECC program [26] and force field [27]; specific parameters for copper(II) bispidine complexes were as used before [1,4]; for Cl[−] the following van der Waals parameters were used: $r_{\text{vdw}} = 1.800$, $\varepsilon = 0.090$. Note that all copper–bispidine parameters are not fully refined.

Ligand field calculations (AOM) were done with CAMMAG [28] and a transferable parameter set (adjusted by 1/(Cu–L) [16], based on normalized Cu–N and Cu–O distances), developed for copper(II) tetra-

mines [17–20]. Parameters for copper(II)–pyridine, copper(II)–acetonitrile and copper(II)–nitrate were adapted from Refs. [22,23] and/or qualitatively fitted to the spectra ($e_{\sigma}^{\text{pyridine}} = 6200$, $e_{\pi}^{\text{pyridine}} = 930$ (for Cu–pyridine = 2.029 Å); $e_{\sigma}^{\text{Cl}} = 5030$, $e_{\pi}^{\text{Cl}} = 900$ (for Cu–Cl = 2.260 Å), $e_{\sigma}^{\text{NCCH}_3} = 4400$, $e_{\pi}^{\text{NCCH}_3} = -100$ (for Cu–NCCH₃ = 1.95 Å), $e_{\sigma}^{\text{NO}_3} = 1417$, $e_{\pi}^{\text{NO}_3} = 250$ (for Cu–NO₃ = 2.440 Å), $e_{\text{ds}} = 1/4 e_{\sigma}$).

DFT-calculations were performed with Gaussian03 [29], using the three-parameter hybrid exchange and correlation functional B3LYP [30,31]. This combination has been demonstrated to provide accurate geometries for a wide range of systems [32] and to perform well with transition metals [33]; various studies have shown it to be a reliable method for copper in all its oxidation states [34–37]. For the geometry optimizations a combination of the 6-311G+(d) basis set (as defined in Gaussian03) for heavy atoms and the 6-31G basis set for H atoms was used (note that the 6-311G command in Gaussian03 corresponds to a combination of basis sets, the Wachters–Hay all electron basis set

for the first transition metal row (i.e. Cu) [38,39], using a scaling factor (with diffuse functions added) [40], the (12s, 9p) (621111, 52111) basis set [41,42] for the second-row main group atoms (i.e. Cl) and the 6-311G basis set [43,44] for first-row atoms (i.e. C, N, O, F). Wavefunction stability tests were run on selected optimized structures. Frequency calculations were performed on all optimized structures to verify their status as true minima on the potential energy surface. For $[\text{Cu}(\text{II})(\text{L})(\text{Cl})]^+$, a single-point energy calculations was performed on the optimized geometry at the B3LYP/6-311G+(3df,2pd) level. This increase in size of the basis set and in the number of polarization functions was found to have a minimal effect on the energy and the energies for the remaining compounds were therefore calculated at the same level of theory as for the geometry optimizations. All energies discussed here are those calculated with the 6-311+G(d) (heavy atoms)/6-31G(H) combination.

Acknowledgements

Generous financial support by the Deutsche Forschungsgemeinschaft (DFG) is gratefully acknowledged.

References

- [1] C. Bleiholder, H. Börzel, P. Comba, A. Heydt, M. Kerscher, S. Kuwata, G. Laurency, G.A. Lawrance, A. Lienke, B. Martin, M. Merz, B. Nuber, H. Pritzkow, accepted.
- [2] P. Comba, R. Ferrari, S. Kuwata, G.A. Lawrance, work in progress.
- [3] P. Comba, W. Schiek, *Coord. Chem. Rev.* 238–239 (2003) 21.
- [4] P. Comba, M. Kerscher, M. Merz, V. Müller, H. Pritzkow, R. Remenyi, W. Schiek, Y. Xiong, *Chem. Eur. J.* 8 (2002) 5750.
- [5] P. Comba, A. Hauser, M. Kerscher, H. Pritzkow, *Angew. Chem.* 115 (2003) 4675.
- [6] P. Comba, M. Kerscher, *Cryst. Eng.* 6 (2004) 197.
- [7] H. Börzel, P. Comba, K.S. Hagen, C. Katsichtis, H. Pritzkow, *Chem. Eur. J.* 6 (2000) 914.
- [8] P. Comba, A. Lienke, *Inorg. Chem.* 40 (2001) 5206.
- [9] P. Comba, M. Merz, H. Pritzkow, *Eur. J. Inorg. Chem.* (2003) 1711.
- [10] M. Bukowski, P. Comba, C. Limberg, M. Merz, L. Que Jr., T. Wistuba, *Angew. Chem.* 116 (2004) 1303.
- [11] H. Börzel, P. Comba, K.S. Hagen, M. Merz, Y.D. Lampeka, A. Lienke, G. Linti, H. Pritzkow, L.V. Tsymbal, *Inorg. Chim. Acta* 337 (2002) 407.
- [12] P. Comba, M. Kerscher, A. Roodt, *Eur. J. Inorg. Chem.* 23 (2004) 4640.
- [13] D. Avnir, P. Comba, S. Keinan (unpublished results).
- [14] D. Wang, G.R. Hanson, *J. Magn. Reson. A* 117 (1995) 1.
- [15] D. Wang, G.R. Hanson, *Appl. Magn. Reson.* 11 (1996) 401.
- [16] B.N. Figgis, M.A. Hitchman, *Ligand Field Theory and its Applications*, Wiley-VCH, 2000.
- [17] P. Comba, T.W. Hambley, M.A. Hitchman, H. Strateimer, *Inorg. Chem.* 34 (1995) 3903.
- [18] P.V. Bernhardt, P. Comba, *Inorg. Chem.* 32 (1993) 2798.
- [19] P. Comba, *Coord. Chem. Rev.* 182 (1999) 343.
- [20] P. Comba, in: J.K.A. Howard, F.H. Allen, G.P. Shields (Eds.), *Implications of Molecular and Materials Structure for New Technologies*, Dordrecht, 1999, p. 87.
- [21] P. Comba, H. Pritzkow, W. Schiek, *Angew. Chem.* 113 (2001) 2556.
- [22] R.G. McDonald, M.J. Riley, M.A. Hitchman, *Inorg. Chem.* 27 (1988) 894.
- [23] T. Astley, P.J. Ellis, H.C. Freeman, M.A. Hitchman, F.R. Keene, E.R.T. Tiekink, *J. Chem. Soc., Dalton Trans.* (1995) 595.
- [24] R. Gleiter, M. Kobayashi, J. Kuthan, *Tetrahedron* 32 (1976) 2775.
- [25] P. Comba, M. Kerscher, H. Pritzkow (work in progress).
- [26] P. Comba, T.W. Hambley, G. Lauer, M. Melter, N. Okon, MOME97, a Molecular Modeling Package for Inorganic Compounds, CVS, 1997.
- [27] J.E. Bol, C. Buning, P. Comba, J. Reedijk, M. Ströhle, *J. Comput. Chem.* 19 (1998) 512.
- [28] M. Gerloch, Cammag, a Fortran Program for AOM calculations, Cambridge, UK, 1991.
- [29] M.J. Frisch, G.W. Trucks, H.B. Schlegel, G.E. Scuseria, M.A. Robb, J.R. Cheeseman, J.A. Montgomery Jr, T. Vreven, K.N. Kudin, J.C. Burant, J.M. Millam, S.S. Iyengar, J. Tomasi, V. Barone, B. Mennucci, M. Cossi, G. Scalmani, N. Rega, G.A. Petersson, H. Nakatsuji, M. Hada, M. Ehara, K. Toyota, R. Fukuda, J. Hasegawa, M. Ishida, T. Nakajima, Y. Honda, O. Kitao, H. Nakai, M. Klene, X. Li, J.E. Knox, H.P. Hratchian, J.B. Cross, V. Bakken, C. Adamo, J. Jaramillo, R. Gomperts, R.E. Stratmann, O. Yazyev, A.J. Austin, R. Cammi, C. Pomelli, J.W. Ochterski, P.Y. Ayala, K. Morokuma, G.A. Voth, P. Salvador, J.J. Dannenberg, V.G. Zakrzewski, S. Dapprich, A.D. Daniels, M.C. Strain, O. Farkas, D.K. Malick, A.D. Rabuck, K. Raghavachari, J.B. Foresman, J.V. Ortiz, Q. Cui, A.G. Baboul, S. Clifford, J. Cioslowski, B.B. Stefanov, G. Liu, A. Liashenko, P. Piskorz, I. Komaromi, R.L. Martin, D.J. Fox, T. Keith, M.A. Al-Laham, C.Y. Peng, A. Nanayakkara, M. Challacombe, P.M.W. Gill, B. Johnson, W. Chen, M.W. Wong, C. Gonzalez, J.A. Pople, in: *Gaussian 03, Revision B.03*, Gaussian, Inc., Wallington CT, USA, 2004.
- [30] C. Lee, W. Yang, R.G. Parr, *Phys. Rev. B* 37 (1988) 785.
- [31] A.D.J. Becke, *J. Chem. Phys. B* 98 (1993) 5648.
- [32] C.W. Bauschlicher, *Chem. Phys. Lett.* 246 (1995) 40.
- [33] S. Nui, M.B. Hall, *Chem. Rev.* 100 (2000) 353.
- [34] M.C. Holthausen, C. Heinemann, H.H. Cornehl, W. Koch, H.J. Schwarz, *J. Chem. Phys.* 102 (1995) 4931.
- [35] A. Ignaczak, J.A.N.F. Gomez, *Chem. Phys. Lett.* 257 (1996) 609.

- [36] L. Rodriguez-Santiago, M. Sodupe, V. Branchadell, *J. Chem. Phys.* 105 (1996) 9966.
- [37] A. Luna, M. Alcami, O. Mo, M. Yanez, *Chem. Phys. Lett.* 320 (2000) 129.
- [38] A.J. Wachtors, *J. Chem. Phys.* 52 (1970) 1033.
- [39] P.J. Hay, *J. Chem. Phys.* 66 (1977) 4377.
- [40] K. Raghavachari, G.W. Trucks, *J. Chem. Phys.* 91 (1989) 1062.
- [41] A.D. McLean, G.S. Chandler, *J. Chem. Phys.* 72 (1980) 5639.
- [42] R. Krishnan, J.S. Binklex, R. Seeger, J.A. Pople, *J. Chem. Phys.* 72 (1980) 650.
- [43] R.C. Binning Jr., L.A. Curtiss, *J. Comp. Chem.* 11 (1990) 1206.
- [44] L.A. Curtiss, M.P. McGrath, J.-P. Blaudeau, N.E. Davis, R.C. Binning Jr., L. Random, *J. Chem. Phys.* 103 (1995) 6104.